Journal of Water Process Engineering 59 (2024) 105079

Contents lists available at ScienceDirect

Journal of Water Process Engineering

journal homepage: www.elsevier.com/locate/jwpe

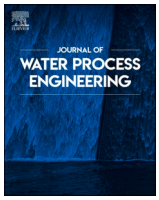

# Phenolic driven decoration of silica with Ag nanoparticles: Towards sustainable water remediation

Marianna Orrico [a], Giulio Pota [a], Virginia Venezia [a,b], Bruno de Gennaro [a], Gianluca Landi [c], Fabiana Tescione [d], Alessandro Pezzella [e], Giuseppina Luciani [a,*], Brigida Silvestri [f,*]

[a] Department of Chemical, Materials and Production Engineering, University of Naples Federico II, Naples, Italy
[b] Department of Structures for Engineering and Architecture, University of Naples Federico II, Naples, Italy
[c] Istituto di Scienze e Tecnologie per l'Energia e la Mobilità Sostenibili STEMS-CNR, Naples, Italy
[d] Institute for Polymers, Composites and Biomaterials (IPCB), CNR, Pozzuoli, NA, Italy
[e] Department of Physics Ettore Pancini, University of Naples Federico II, Naples, Italy
[f] Department of Civil, Architectural and Environmental Engineering, University of Naples Federico II, Naples, Italy

ARTICLE INFO

Editor: Tzyy Haur Chong

*Keywords:*
5,6-Dihydroxyindole-2-carboxylic acid
Bio-available caffeic and gallic acid
Hybrid silica based nanocatalysts
Organic dyes removal
Water remediation

ABSTRACT

The development of effective systems for the removal of toxic compounds from wastewater is an important goal in the production of materials for environmental applications. In this work we report a sustainable approach for the design and development of silver-decorated hybrid silica nanoparticles for the adsorption and catalytic degradation of toxic dyes. Different bio-available and inexpensive phenolic precursors were selected to chelate and reduce silver ions, and the final nanoparticles architecture was modified by exploring two different synthesis strategies. In the first route, silica nanoparticles were formed in a solution containing both phenolic and metallic components, whereas, in the second route, silver ions were added in an environment where hybrid nanoparticles have already been formed.

It was shown that the appropriate choice of both phenolic component and the synthetic route can strongly influence the catalytic activity towards dye degradation. Indeed, the proposed systems show almost complete degradation and reduction of Methylene Blue and 4-Nitrophenol, depending on the exposure and stability of the silver metal active sites.

## 1. Introduction

Access to potable and unpolluted water is a top priority goal in light of modern society development and the exponential rise of industry. One of the major environmental issues is the contamination of water resources caused by contaminants such as organic dyes released by textile, food, printing paper, pharmaceutical, and cosmetic industries [1–5]. In this context, the textile industry has a significant impact on the environment, both in terms of natural resource exploitation and contaminant release. 400 billion square meters of fabric require nine trillion liters of water, six of which are used for dyeing [6,7]. Furthermore, textile treatments and synthetic dyes are responsible for 20 % of global pollution of clear water [8,9]. Compared to natural ones, synthetic dyes have the advantage of being less expensive and having an excellent affinity with synthetic fibers such as nylon, viscose, and polyester. However, they are not only bio-accumulative and persistent in the environment, but also toxic to the ecosystem and humans due to their complex chemical structures, which are typically alkylphenols, azo compounds, and chlorobenzenes. In addition, they are designed to be resistant to common oxidation and reduction processes, thus extremely difficult to remove from textile industry wastewater. Several methods have been suggested for removing toxic compounds from wastewater, including coagulation/flocculation [10], advanced oxidative processes [11], biological treatment [12], solvent extraction [13], distillation [14] and membrane filtration [15]. These processes are expensive because of the high energy requirements, instead, adsorption/catalytic reduction is widely accepted and preferred method as simple and effective strategy [16–18]. In this context, the adsorption and catalytic reduction of dyes

* Corresponding authors.
*E-mail addresses:* marianna.orrico@unina.it (M. Orrico), giulio.pota@unina.it (G. Pota), virginia.venezia@unina.it (V. Venezia), brdegenn@unina.it (B. de Gennaro), gianluca.landi@stems.cnr.it (G. Landi), fabiana.tescione@cnr.it (F. Tescione), alessandro.pezzella@unina.it (A. Pezzella), luciani@unina.it (G. Luciani), brigida.silvestri@unina.it (B. Silvestri).

https://doi.org/10.1016/j.jwpe.2024.105079
Received 14 December 2023; Received in revised form 8 February 2024; Accepted 26 February 2024
Available online 2 March 2024

and, more generally, of emerging organic pollutants, has gained increasing attention in recent years [19–24]. To this regard, metal nanoparticles represent ideal candidates in reductive degradation of harmful and toxic dyes due to their unique physical and chemical features strictly related to their size and morphology [25–32]. In addition, the adoption of sustainable practices using green chemistry is gaining prominence as an essential strategy to enhance and safeguard our global environment. This approach is a focal point in various research fields, aimed at improving and preserving our planet for the future. In this scenario, there has been a growing focus on the green synthesis route of metal nanoparticles [33–35]. Instead of using harmful chemicals to reduce and stabilize metallic nanoparticles, different bio-wastes are emerging as a promising low-cost source of multifunctional compounds with redox activity. These bio-wastes include polyphenolic and polyhydroxindole moieties, which show a promising ability in effectively chelating and reducing metal ions [36–46]. Furthermore, combining these bio-derived compounds with a nanostructured inorganic phase may improve their stability as well as their functional properties [47,48]. To this regard, we recently demonstrated the possibility of improving the inherent characteristics of melanin-like materials using templated polymerization of 5,6-dihydroxyindole-2-carboxylic acid (DHICA) in the presence of silica phase. Among the various inorganic components, silica has proved to be an extremely versatile templating agent for obtaining nanoparticles with tunable size and surface chemistry, and tailored performance for a wide range of applications [49–52]. Following a sustainable approach, in this work the ceramic templated approach is synergistically integrated with the red-ox properties of polyphenolic compounds in order to develop polyphenol-based nanocatalysts for the adsorption and the catalytic reduction of toxic dyes from urban and industrial wastewater. Notably the current study aims at: (1) exploring bio-available caffeic acid and gallic acid as potential melanogenic precursors and Ag reducing agent, (2) comparing the obtained hybrid structures with those based on DHICA-derived melanin, (3) analyzing the impact of two different synthesis strategies on the final system catalytic efficiency. The hybrid systems were tested for adsorption and catalytic reduction of model pollutants Methylene Blue (MB) and 4-Nitrophenol (4-NP). The results demonstrated distinct performances based on the hybrid system architectures.

## 2. Materials and methods

### 2.1. Materials

N-(3-Dimethylaminopropyl)-N′-ethyl-Carbodiimide hydrochloride (EDC, protein seq. grade), N-Hydroxy Succinimide (NHS, 98 %), 3-(Aminopropyl) Triethoxy Silane (APTS), Tetra Ethyl Orthosilicate metal basis (TEOS, 99.999 %), ammonium hydroxide (ACS reagents, 28.0-30.0 %$NH_3$), Ethanol (absolute, ≥99.8 %), Silver nitrate (99.9999 %), Methylene Blue (3,7-bis (*N*, *N*-dimethylamino) phenothiazinium chloride), 4-Nitrophenol, Gallic acid (trihydroxybenzoic acid) and Caffeic acid (3- (3,4-dihydroxyphenyl) prop-2E-enoic acid) were purchased from Sigma-Aldrich (St Louis, MO, USA) and used as received. DHICA monomer was prepared as described elsewhere [36].

### 2.2. Preparation of hybrid nanoparticles

The hybrid nanoparticles were synthesized following an in situ sol-gel procedure, by making slight modifications to a tried and tested procedure [50,51]. Accordingly, the APTS-melanogenic hybrid precursors were first synthesized overnight via EDC/NHS chemistry, using DHICA, CAF and GAL. Subsequently, using a modified Stober method, hybrid nanoparticles were prepared [49]. Two different synthesis strategies were here explored and schematically described in Scheme 1:

- Procedure 1

Silver nitrate was added immediately before TEOS addition. In this case, hybrid nanoparticles were formed in a solution containing both organic and metallic components. These samples will be indicated in the following as DHICA-Ag_1, CAF-Ag_1 and GAL-Ag_1.

- Procedure 2

Silver nitrate was added after 18 h from TEOS addition. These samples will be indicated in the following as DHICA-Ag_2, CAF-Ag_2 and GAL-Ag_2.

At the end of each described procedure, the nanoparticles were recovered by centrifugation and repeatedly washed for 3 times using distilled water.

### 2.3. Physical-chemical characterization

Nanoparticles morphology was studied using Transmission Electron Microscopy (TEM). Briefly, aqueous solution of nanoparticles was dispersed on a copper grid (200 mesh with carbon membrane). TEM pictures were captured using a TECNAI 20 G2: FEI Company (Eagle 2HS camera). The images were acquired at a voltage of 200 kV, with a camera exposure time of 1 s and a size of 2048 × 2048. Thermogravimetric analysis (TGA) was carried out using a TA Instrument thermoanalyser SDT Q600 (TA Instrument, New Castle, DE, USA) to study the thermal behavior of obtained samples. Approximately 15 mg of each sample were tested under a nitrogen atmosphere, with a heating rate of

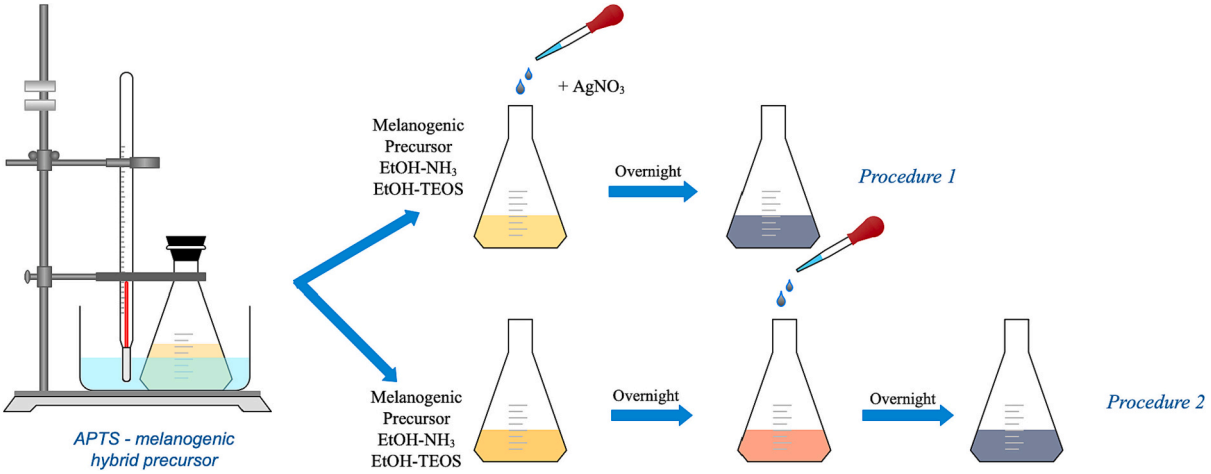


**Scheme 1.** Schematic presentation of the procedures for synthesizing hybrid nanoparticles.

10 °C/min. ζ-Potential experiments were carried out using a Zetasizer equipment (Nanoseries, Malvern) to evaluate the surface charge of obtained nanoparticles. All samples were diluted to a droplet concentration of around 0.025 % w/v and the analyses were performed by executing 50 runs for each measurement. The FT-IR spectra were acquired using a Nexus FT-IR spectrometer to unveil the chemical composition of obtained nanoparticles. By dispersing 0.5 mg of the nanoparticles in KBr, 200 mg pellets were formed, and all spectra were recorded in the 4000–400 $cm^{-1}$ range, with a resolution of 2 $cm^{-1}$. $N_2$ adsorption was used to determine the BET specific surface areas (SSA) of nanoparticles using a Quantachrome Autosorb-1C equipment. All samples were degassed for 3 h at 150 °C. The silver content of all synthesized samples was determined using Plasma Emission Spectrophotometry, ICP-OES Perkin-Elmer Optima 2100DV. Each system was digested in 10 mL of an acid mixture of $HNO_3$, HCl, and HF. All tests were performed in triplicate. Finally, the Ultraviolet-Visible (UV visible) spectroscopic studies were carried out on a SHIMADZU UV-2600i spectrophotometer (Shimadzu, Milan, Italy).

### 2.4. Adsorption and catalytic reduction of MB

To investigate the adsorption capacity of as-prepared nanoparticles, 2.5 mg of each catalyst were dispersed in 12.5 mL of an aqueous solution containing $5 \times 10^{-3}$ mM of MB for 30 min in the dark. Nanoparticles were then separated by centrifugation and the adsorbent free solution was collected for analysis. The adsorption efficiency of MB was determined on the base of UV–Vis measurements, at the $\lambda_{max}$ value of 664 nm, by using the Eq. (1):

$$\eta(\%) = \frac{C_0 - C_e}{C_0} \cdot 100 \quad (1)$$

where $C_0$ is the initial concentration of MB and $C_e$ the MB concentration in the supernatants after 30′ of adsorption step. In addition, after the adsorption step, nanoparticles were resuspended in 12.5 mL of distilled water and the performance in reduction of the adsorbed MB was evaluated by adding 3.0 mL of $NaBH_4$ aqueous solution (0.01 M). The presence of eventually residual MB was assessed by collecting the UV–Vis spectra of nanoparticles suspension before and after the addition of $NaBH_4$. After the reactions were completed, the nanoparticles were removed from the reduction reaction media, washed with water, and reused in the next catalytic cycle.

### 2.5. Catalytic reduction of 4-NP to 4-AP

The catalytic activity of all samples was also investigated in the reduction reaction of 4-NP to aminophenol (4-AP). To this aim, a mixture of 10 mL of aqueous solution of 4-NP (2 mM) and 5 mL of aqueous solution of $NaBH_4$ (0.25 M) were prepared and analyzed through UV–Vis spectrometer. Then, 2 mg of nanoparticles were added to this solution and the progress of reduction reaction was monitored by the evolution of the UV–Vis spectra over time.

The Turnover Frequency (TOF) of each sample was calculated. To this purpose, a pseudo-first-order kinetic constant was considered, since it proper fits the catalytic performance. Then, TOF was calculated according to Eq. (2):

$$TOF = \frac{k \cdot n^0}{n_{Ag}} \quad (2)$$

where k is the pseudo-first-order kinetic constant ($s^{-1}$), $n^0$ is the initial amount of 4-NP (mol), and $n_{Ag}$ is the actual amount of silver (mol).

## 3. Results and discussion

### 3.1. Characterization of the hybrid nanostructures

Fig. 1 reports the XRD patterns of the synthesized samples. In all spectra, a broad band ranging from 15° to 30° in 2θ angle is evident, thus suggesting the amorphous nature of silica skeleton. Additionally, four distinct diffraction peaks can be observed at 2θ = 38°, 44°, 64°, and 77°. These peaks were assigned to (111), (200), (220), and (311) planes, indicating the presence of Ag(0) crystals with face centered cubic (FCC) structure in the hybrid nanostructures [30,53,54]. Therefore, these findings confirm the reduction of silver ions during the synthesis and suggest the key role of phenolic components as reducing agents in accordance with previously reported studies [55,56].

The samples were analyzed by ICP-EOS to determine the Ag contents, as reported in the Table 1.

The obtained results reveal that all samples have a comparable total Ag amount, swinging around 30 μg/mg, with the exception of sample DHICA-Ag_2, which show approximately 40 μg/mg. The morphology of all synthesized samples was examined by TEM analysis. Fig. 2 shows TEM images and the size distribution of Ag clusters of DHICA-Ag_1 (a), CAF-Ag_1 (b), GAL-Ag_1 (c), DHICA-Ag_2 (d), CAF-Ag_2 (e) and GAL-Ag_2 (f) nanoparticles. Different contrast areas could be seen in all samples: small black areas, attributed to the metallic Ag domains, and pseudo-spherical less dense larger particles with rough surfaces, corresponding to the polyphenol/silica hybrid domains. In particular, DHICA-Ag_1 samples exhibit a core-shell architecture made of a darker metal core wrapped by a lighter hybrid silica domain, on the other hand DHICA-Ag_2 nanoparticles evidence a different architecture with silver clusters preferentially located on the surface (Fig. 2d). Thus, from the analysis of TEM features it can be inferred that the synthesis procedure and in particular the order of DHICA and TEOS addition in the synthesis batch strongly affect the structure of the final system.

More specifically, for both synthesis procedures, the reaction mixture quickly turns black immediately after the addition of $AgNO_3$ when DHICA monomer is used (Fig. 2(a) and (d)), suggesting the occurrence of DHICA oxidative polymerization and concurrent reduction of silver ions. For DHICA-Ag_1 sample, these processes produced a relevant fraction of hybrid melanin-silver clusters, with an average diameter of approximately 20 nm, which acted as nucleation sites for subsequent silica shell formation, resulting in a final core shell architecture (Fig. 2a) [49]. On the other hand, for DHICA-Ag_2 sample, since TEOS is added before DHICA, silica formation is triggered before DHICA polymerization. Accordingly, the reduction of silver ions must occur on

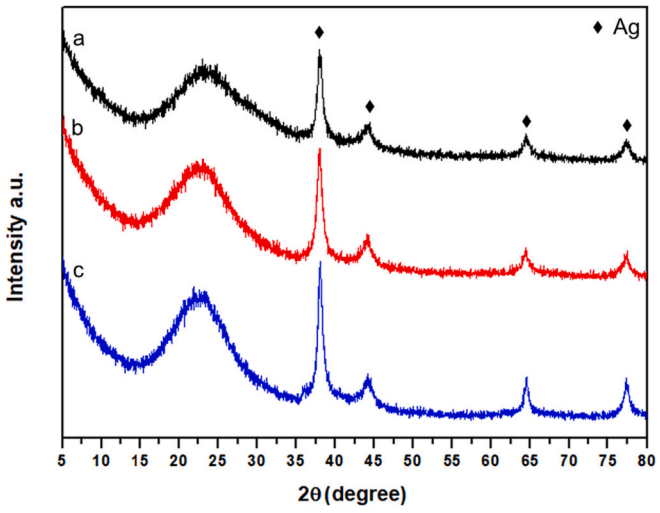


**Fig. 1.** XRD patterns of DHICA-Ag (a), CAF-Ag (b) and GAL-Ag (c) samples, representative of both synthesis procedures.

**Table 1**
Ag concentration (as μm of silver per mg of nanoparticles) by ICP-OES analysis.

| Sample | Ag amount (μg/mg) |
|---|---|
| DHICA-Ag_1 | 27.5 ± 1.4 |
| CAF-Ag_1 | 29.7 ± 1.5 |
| GAL-Ag_1 | 31.8 ± 1.6 |
| DHICA-Ag_2 | 39.7 ± 1.8 |
| CAF-Ag_2 | 30.7 ± 1.6 |
| GAL-Ag_2 | 32.4 ± 1.4 |

the surface of already formed hybrid nanoparticles where hybrid APTS-DHICA domains are probably more exposed. Thus, dark melanin-silver clusters with a mean diameter of 15 nm, are clearly visible on the surface of the particles (Fig. 2d). A different morphology can be observed in the case of all CAF-Ag and Gal-Ag samples (Fig. 2(b), (e) and (c), (f), respectively). Particularly, TEM micrographs show small silver clusters uniformly dispersed onto the surface of hybrid nanoparticles. On the surface of CAF-Ag_1 nanoparticles (Fig. 2(b)), Ag domains of about 2,5 nm in diameter were found. Except for the appearance of larger black dots (of about 7 nm in diameter), the morphology of CAF-Ag_2 NPs looked quite close to that of CAF-Ag_1 nanoparticles (Fig. 2(e)). Finally, similar structures were observed in TEM micrographs of both GAL-Ag samples, with the size distribution of Ag clusters showing an average diameter of about 4–5 nm (Fig. 2(c) and (f)), only a significant decrease in the number of Ag nanoparticles with respect to CAF-Ag samples can be appreciated. Indeed, during the synthesis of these samples (CAF-Ag and GAL-Ag), the solution gradually became opalescent and gray with the addition of silver salt, suggesting a slower $Ag^{+}$ ions reduction into metal Ag(0) and, concurrently, slower phenolic acid oxidation than DHICA. Therefore, it is reasonable to assume that when caffeic and gallic acids are used in procedure 1, silica formation may occur before metal reduction, resulting in the formation of small Ag(0) domains mainly located on the surface of preformed silica particles. This might be due to the presence of more exposed phenolic groups than DHICA. These hypotheses were supported by surface charge measurement and Folin-Ciocâlteu assay (Table 2) which reveal precious information on the chemistry of the exposed groups, thus justifying the functionality of each sample. Firstly, nanoparticles synthesized from DHICA monomer showed marked differences in the surface charge values depending on the synthesis procedure. Following the procedure 1 (where silver nitrate was added immediately before silica precursor addition), a ζ-potential value of −12.30 mV (DHICA-Ag_1) was detected, while the procedure 2 (where silver nitrate was added after 18 h from silica precursor addition) led to a significant decrease in the surface charge of the particles which showed a ζ-potential value of about −60.00 mV (DHICA-Ag_2). On the other hand, CAF-Ag and GAL-Ag nanoparticles exhibited comparable values of the ζ-Potential (~−45.00 mV) and only a slight decrease was observed (~−22.00 mV) when they are synthesized following the procedure 2. The different surface charge is probably due to a different exposure of phenolic groups, as shown by the results of Folin-Ciocâlteu assay, reported in the Table 2. DHICA-Ag_1 had a lower concentration of exposed phenolic groups with respect to both CAF-Ag_1 and GAL-Ag_1 samples. In contrast, DHICA-Ag_2 sample exhibited the largest amount of surface phenolic groups. These results support the hypothesis of a different surface organization of organic and inorganic components, enabling a distinct distribution of metal domains in the final nanoparticles. Indeed, three different processes are in competition: (i) the hydrolysis and condensation reactions forming the inorganic silica phase, (ii) phenolic acid oxidation/polymerization, and (iii) the reduction of silver ions to metal silver by phenolic groups. The appropriate choice of silver addition, immediately before or 18 h after TEOS addition, allows for tuning the final nanoparticles architecture. Following procedure 1, when DHICA monomer was used, oxidation/polymerization and reduction reactions proceed concurrently and rapidly enough to occur before silica formation. Therefore, silver-phenolic domains acted as nucleation sites for subsequent silica formations. On the other hand, the preformed silica particles in procedure 2 might promote the formation metallic domains on the surface, where the phenolic groups are more exposed. Such diverse architectures are not achievable with caffeic and gallic acid monomers, since gained results suggest that the oxidation-polymerization/reduction kinetics are slower than DHICA and cannot compete with silica formation. For these reasons, the final architecture is not influenced by the addition order of organic and inorganic precursors and both procedures led to the formation of silver domains on the particle surface. The organic fraction content in hybrid nanoparticles and ascribable to the polyphenol chains, was estimated using TGA analysis (Fig. S1), which revealed a different profile for each sample. The removal of physically adsorbed water is responsible for the first weight loss within 100 °C. Additional weight loss in the range 200–650 °C, can be attributed to the decomposition of the organic component. The estimated organic amount based on TGA analysis is reported in the Table 2 [57]. The specific surface area of all nanoparticles was calculated from $N_2$ adsorption/desorption isotherms, using the BET method and the Table 2 summarizes the obtained results. Both DHICA-Ag_1 and GAL-Ag_1 samples showed the highest specific surface area values, which slightly decreased in DHICA-Ag_2 and GAL-Ag_2 samples. In the case of CAF-Ag_1 and CAF-Ag_2 samples, no significant SSA differences were observed using the two different synthesis procedures. Furthermore, the FTIR analysis reported in Fig. S2 and representative of all analyzed samples, showed the typical absorption bands of silica gel phase [58,59].

### 3.2. Catalytic tests and operational stability assessment

#### 3.2.1. MB adsorption and degradation

In order to evaluate the adsorption capacity, all samples were soaked into a MB aqueous solution, as described in the experimental section and the MB uptake was measured by UV–Vis analysis. Fig. 3 shows the UV–Vis spectra of the supernatants obtained from centrifugation of each sample after 30 min of soaking into MB solution. The adsorption spectrum of bare MB solution has been used as comparison.

The reduction in the typical adsorption peak of MB at 664 nm demonstrated a good adsorption capacity towards MB of all samples, because of the electrostatic interactions between the negatively charged surface of particles (as indicated in the Table 2 for ζ-potentials) and the positively charged MB. Furthermore, no significant changes in the UV–Vis spectra are observed for samples synthesized using the procedure 1 (Fig. 3a). On the other hand, better adsorption performances were observed for DHICA-Ag_2 and COF-Ag_2 samples prepared using the procedure 2 (Fig. 3b), with the complete disappearance of typical MB peaks when using DHICA-Ag_2 sample. The high adsorption capacity exhibited by this last sample can be explained by its significantly higher negative charge, coupled with a larger availability of exposed phenols, with respect to those of other synthesized systems [60]. MB adsorption efficiency, calculated using Eq. (1), was reported in the Fig. 4 which clearly shows that both DHICA-Ag_2 and CAF-Ag_2 samples exhibited significantly higher dye adsorption efficiency, reaching value of about 100 and 80 % of MB removal percentage, respectively. On the other hand, no apparent variations in adsorption capacity occur between GAL-Ag_1 and GAL-Ag_2 samples.

The adsorbent desorption and, therefore, the system reusability represent key factors in economically treating wastewater. Regeneration of nanoparticles was carried out by the reduction of MB through $NaBH_4$. After MB adsorption, all samples were collected by centrifugation, and resuspended in aqueous media, and then $NaBH_4$ solution was added to obtain MB degradation. After the reactions were completed, the nanoparticles were removed from the reaction media, washed with water, and reused for five consecutive cycles.

Fig. 5 reports images of suspensions containing the DHICA-Ag_1, CAF-Ag_1, and GAL-Ag_1 nanoparticles after MB adsorption, before (Fig. 5a1, a2, a3) and immediately after (Fig. 5b1, b2, b3) the addition of

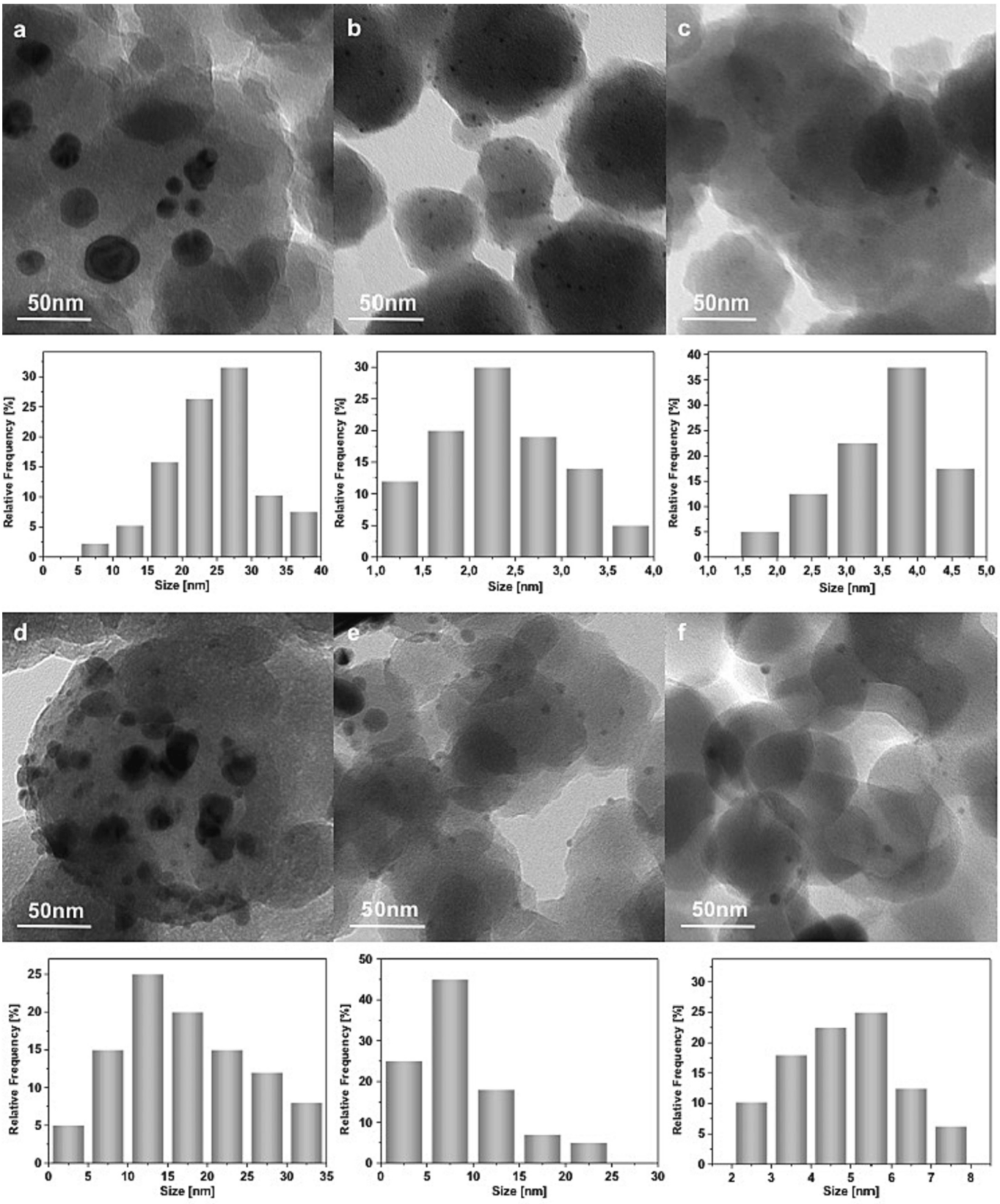


**Fig. 2.** TEM images of prepared samples: DHICA-Ag_1 (a), CAF-Ag_1 (b), GAL-Ag_1 (c), DHICA-Ag_2 (d), CAF-Ag_2 (e), GAL-Ag_2 (f) and relative graphs showing the size distribution of Ag clusters.

**Table 2**
Organic content estimated from TG analysis, Specific Surface Area, Zeta Potential and Folin-Ciocâlteu assay results.

| Samples | Organic content (%) | Specific Surface Area SSA ($m^2/g$) (±4 %) | ζ-Potential (mV) | Equivalent gallic acid/sample (mg/g) |
|---|---|---|---|---|
| DHICA-Ag_1 | 10.0 ± 0.7 | 79.0 | −12.3 ± 0.65 | 230 ± 20 |
| CAF-Ag_1 | 4.38 ± 1.1 | 55.0 | −46.4 ± 1.47 | 325 ± 15 |
| GAL-Ag_1 | 6.04 ± 0.6 | 65.5 | −46.1 ± 1.21 | 283 ± 15 |
| DHICA-Ag_2 | 12.0 ± 0.8 | 65.5 | −60.0 ± 0.73 | 436 ± 11 |
| CAF-Ag_2 | 11.1 ± 1.3 | 55.0 | −21.3 ± 0.95 | 254 ± 18 |
| GAL-Ag_2 | 6.37 ± 1.2 | 59.8 | −24.2 ± 1.34 | 337 ± 10 |

the reducing agent.

In the case of CAF-Ag_1 and GAL-Ag_1 samples (Fig. 5a2, a3), the dye characteristic blue color is visible in the nanoparticles aqueous suspension. However, immediately after the addition of $NaBH_4$, the suspensions become colorless. On the other hand, for DHICA-Ag_1 sample (Fig. 5a1), the blue color of the suspension is potentially masked by the darker appearance characteristic of the nanoparticles themselves, which have a darker color after synthesis compared to the other samples. Nevertheless, even in this case, a fading in the suspension color is noticeable after the addition of the reducing agent. Qualitative observation is supported by UV–Vis analysis. Indeed, Fig. 5c reports the UV–Vis spectra of bare nanoparticles (black curve), the nanoparticles after the adsorption step (blue curve) and after $NaBH_4$ addition (red curve), which are representative for all analyzed systems. In particular, UV–Vis spectra of nanoparticle suspension after the adsorption step show the typical adsorption peak of MB at 664, thus confirming its presence in the nanoparticles. This peak is no longer evident in the presence of $NaBH_4$ suggesting that a reaction occurred between MB and $NaBH_4$. In the presence of $NaBH_4$ reducing agent and metal component as catalyst, an electron transfer mechanism can be considered to explain MB reduction process. Specifically, silver is a good conductor and can facilitate electron transfer between the donor ($BH_4^-$) and the acceptor (MB) promoting the reduction of MB to Leucomethylene Blue (LMB) (Fig. 6), which spontaneously desorbs from the surface of the nanoparticles, turning the solution that was originally vivid blue to colorless [60,61].

Finally, to assess their reusability, the utilized nanoparticles were isolated, through centrifugation, from the reaction mixtures and reused in subsequent cycles for MB adsorption. The obtained results are reported in the Fig. 7.

DHICA-Ag and GAL-Ag samples obtained from both synthesis

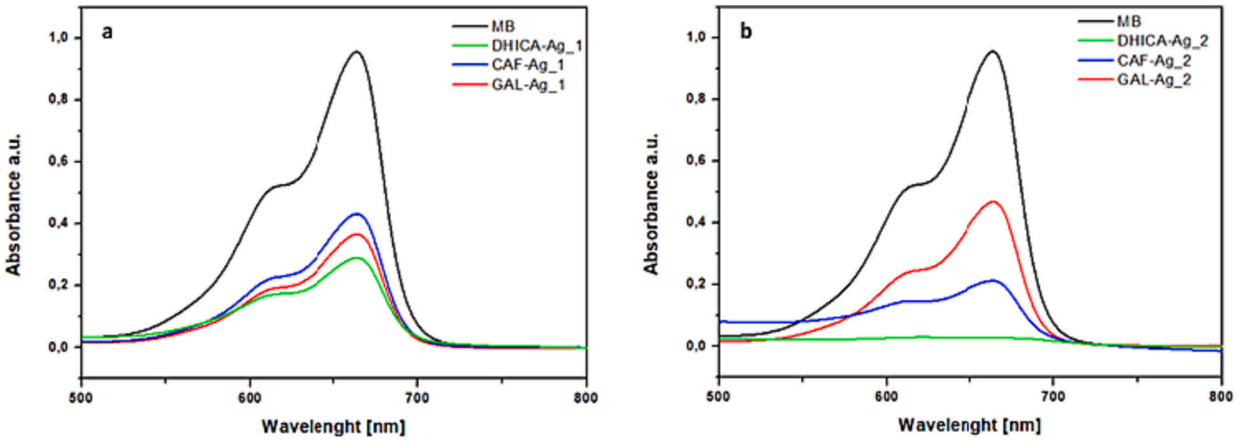


**Fig. 3.** UV–Vis spectra of the supernatants of samples produced by procedure 1 (a) and procedure 2 (b).

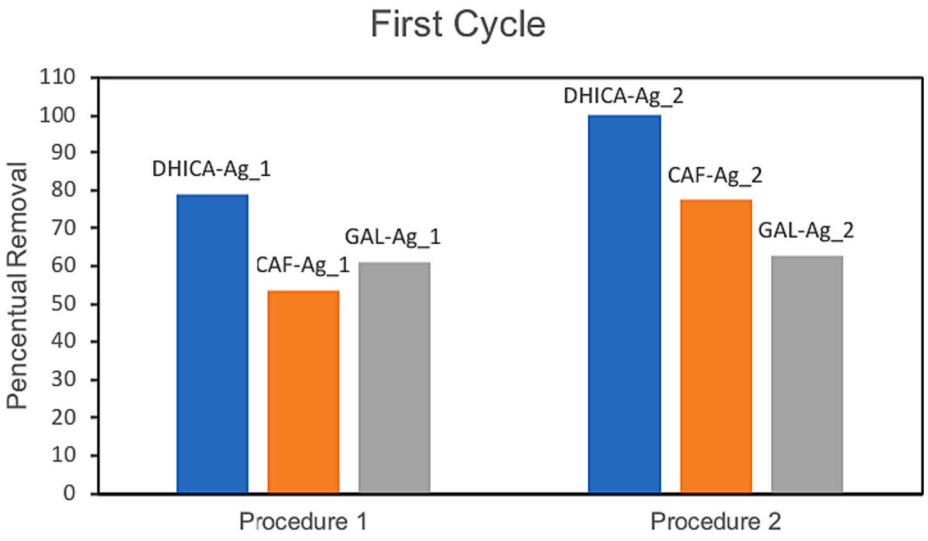


**Fig. 4.** MB adsorption efficiency of all investigated samples. Experiments were performed in triplicate and as much as 5 % error was detected.

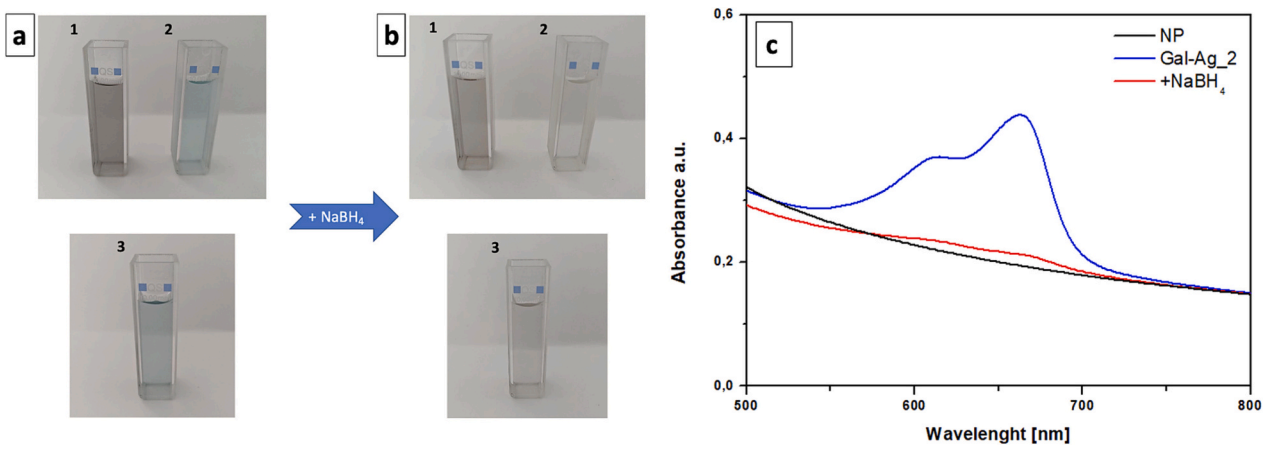


**Fig. 5.** Aqueous suspensions of DHICA-Ag_1, CAF-Ag_1, and GAL-Ag_1 nanoparticles containing MB before (a1, a2, a3) and after (b1, b2, b3) the addition of $NaBH_4$ and UV–Vis representative spectra (c) of the bare nanoparticles (black curve), nanoparticles containing MB before (blue curve) and after (red curve) $NaBH_4$ addition.

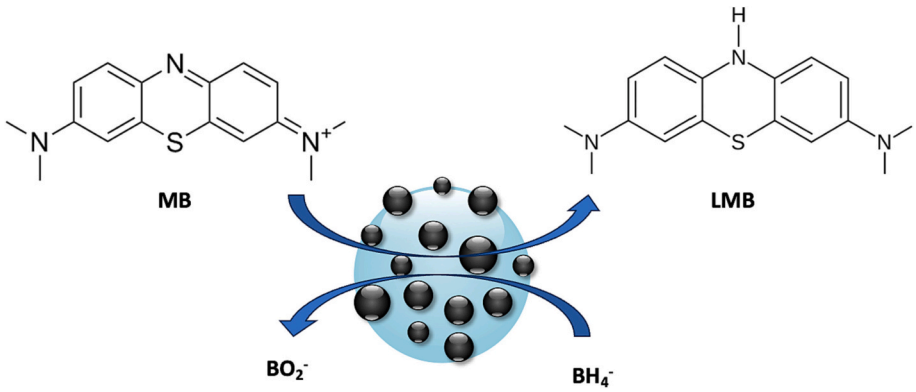


**Fig. 6.** Reduction mechanism of MB in the presence of nanoparticles.

procedures exhibit good recyclability, especially for DHICA-Ag_2 sample, while in the case of CAF-Ag samples, a certain deactivation is observed starting from the second cycle, suggesting a significant reduction in MB content adsorbed. Interestingly, among all samples, DHICA-Ag_2 exhibited better dye removal and high reusability performance.

### 3.2.2. *Reduction test of 4-Nitrophenol to 4-Aminophenol*

The catalytic performances of all synthesized samples were also investigated in the reduction reaction of 4-NP to 4-AP in the presence of an excess of $NaBH_4$, as described in Section 2.5 of the Experimental section. This process involves two steps: the formation of Nitrophenolate ion followed by the reduction to aminophenol. The UV–Vis spectrum of 4-NP (Fig. 8. Black curve), exhibits the main characteristic absorption peak at around 310 nm. The introduction of $NaBH_4$ reducing agent induces a red-shift in absorption maximum from 310 nm to around 400 nm, due to the formation of the 4-Nitrophenolate ($4\text{-}NP^-$) ion. Moreover, in the absence of a catalyst, this peak remains unchanged [61,62].

In addition, the formation of the 4-Nitrophenolate ion also resulted in a markedly color change of the solution from light to bright yellow, as evidenced in the picture inserted in the Fig. 8. To explore the catalytic properties of the synthesized systems in the reduction reaction of 4-NP to 4-AP, 2 mg of each catalyst were introduced into the solutions containing the 4-Nitrophenolate ion. After nanoparticles addition to the system, a rapid color change in the solution is immediately observed. Indeed, in all systems, the bright yellow color fades and the solution turns darker in the case of both DHICA-Ag samples (due to the presence of nanoparticles with a much darker color than the others) and completely colorless in the case of the CAF-Ag and GAL-Ag samples, as shown in the Fig. S3. UV–Vis analysis was used to follow the reduction reaction of 4-NP to 4-AP over time due to the catalytic properties of the synthesized systems (Fig. 9).

The UV–Vis spectra of Fig. 9 clearly show the disappearance of the peak at 400 nm and the simultaneous appearance of a new absorption peak at around 300 nm, ascribable to 4-AP production. Furthermore, the absence of additional peaks in the absorption spectra suggests that the reduction of 4-NP to 4-AP does not produce any undesirable by-products [61–64]. All samples show almost complete reduction with different times. Notably, DHICA-Ag_2 and CAF-Ag_2 samples showed faster reduction reaction times as the signal at 400 nm totally disappeared after only 4 min of the reaction, leaving only the peak at around 300 nm associated to 4-AP production. In addition, the reduction of 4-NP to 4-AP occurs instantly in the case of CAF-Ag_1 sample, even making difficult its detection in absorption spectra. Both GAL-Ag_1 and GAL-Ag_2 samples exhibited a very similar behavior, with degradation times of approximately 27 min. Finally, DHICA-Ag_1 demonstrated the longest degradation time, taking about 50 min for the complete reduction.

Fig. 10 shows the TOFs of the different samples, calculated according to the procedure reported in Section 2.4. It is worth noting that a good fit is achieved using first-order kinetics. In the case of CAF-Ag1 sample kinetics are extremely fast, and complete conversion was appreciated after 2 min. The calculated rate constant corresponds to achieving 100 % conversion in 2 min, even though it could be achieved sooner. The exceptional activity of CAF-Ag1 appears clearly by comparing TOFs; as a matter of fact, its intrinsic activity is at least four times as high as those of the other samples. By excluding CAF samples, procedure 2 provides

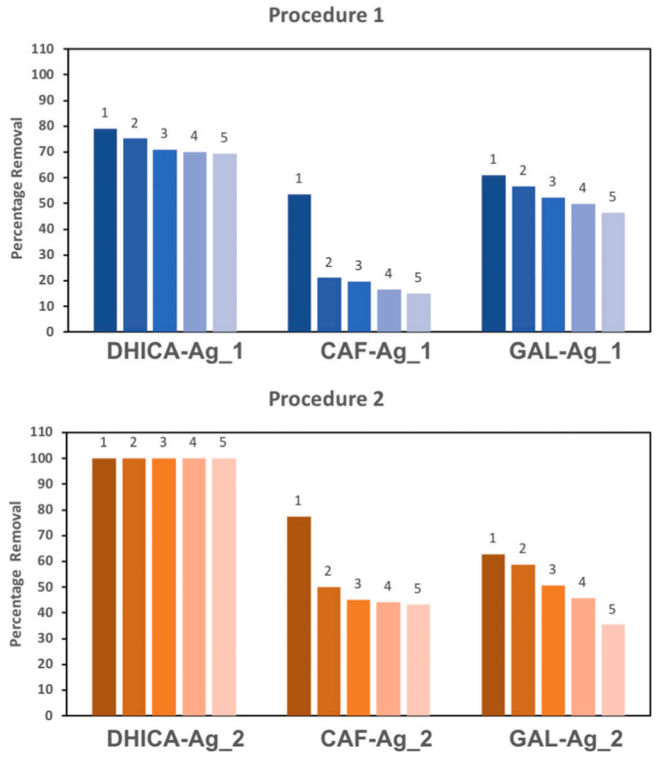


**Fig. 7.** MB percentage removal of all investigated samples for 5 cycles. Experiments were run in triplicate and as much as 5 % error was detected.

better-performing materials.

The different catalytic behaviors of the samples can be attributed to the different distribution and availability of silver domains, which are bound to act as active sites for red-ox reaction is located within these active domains, between $BH_4^-$ ions (donor) and the dye (acceptor). As a result of electron transfer, hydrogenation of 4-NP occurs, leading to the spontaneous desorption of the reduction product (4-AP), ultimately allowing the active sites available for a new reduction event [61]. Fig. 11 shows a representative scheme of the reduction reaction of 4-Nitrophenol to 4-Aminophenol.

Given the same silver amount in all samples, the availability and the accessibility of metal silver improve the efficacy of the catalytic process, thus allowing for a faster reduction rate in samples with higher exposure of active silver sites. As evidenced in TEM micrographs, in DHICA-Ag_2, CAF-Ag_1, and CAF-Ag_2 samples (Fig. 2d, b and e), the active silver sites are more exposed since available on the surface, thus the reduction process of 4-NP occurs at a faster rate than DHICA-Ag_1 and both Gal-Ag samples. Furthermore, the exceptional catalytic activity of CAF-Ag_1 sample, exhibiting the highest TOF value (Fig. 10), can be related to the highly dispersed and small size of silver clusters available on the surface, as evidenced by TEM investigation (Fig. 2b). The slower reduction rate observed for GAL-based systems is likely due to the lower presence of silver domains on the surface of the hybrid particles. This reduced availability of active sites on the surface could result in a slower catalytic reaction for the reduction of 4-NP to 4-AP. Finally, in the case of the DHICA-Ag_1 sample, the longer reaction times can be explained by its unique architecture, which differs from all other synthesized nanocatalysts. As evidenced in TEM micrograph (Fig. 2a) the metallic Ag phase is segregated within the nanoparticle core. As a result, a preliminary stage of 4-NP diffusion within the nanoparticles is expected. The reduction reaction occur only after the metallic active site is reached, resulting in the release of 4-AP [23,60]. A comparison with similar silver-based nanocatalyst of MB removal capacity for MB and 4-NP reduction reaction, reported in Tables S1 and S2, respectively, confirmed the good activities of here proposed systems. The reduction reaction efficiency of 4-NP in the presence of nanoparticles was investigated for 5 consecutive cycles. Fig. 12 shows the time required for the complete disappearance of the peak at 400 nm in each reuse cycle for all investigated samples.

All samples achieve complete reduction of 4-NP to 4-AP. Among the samples prepared following procedure 1, both CAF-Ag_1 and GAL-Ag_1 samples showed a gradual increase in total reduction reaction times with increasing reuse cycle, while a unique behavior was observed for DHICA-Ag_1 (Fig. 12a, red curve), which showed a remarkable reduction in reaction time as it is reused. For samples synthesized following the procedure 2 (Fig. 12b), both DHICA-Ag_2 and CAF-Ag_2 samples

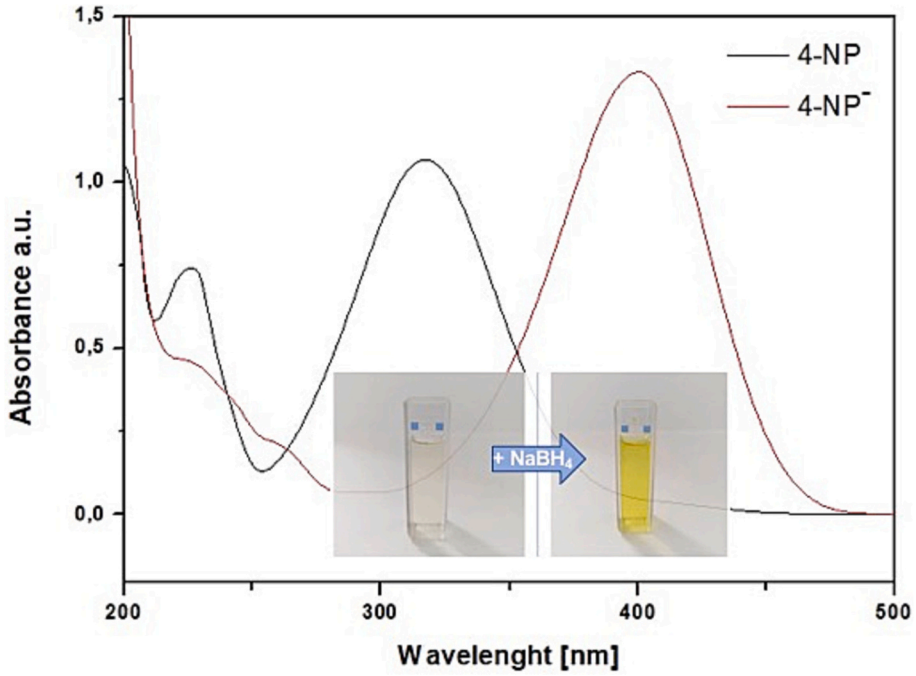


**Fig. 8.** UV–Vis spectra for catalytic reduction of 4-Nitrophenol to 4-Nitrophenolate ion in the presence of $NaBH_4$.

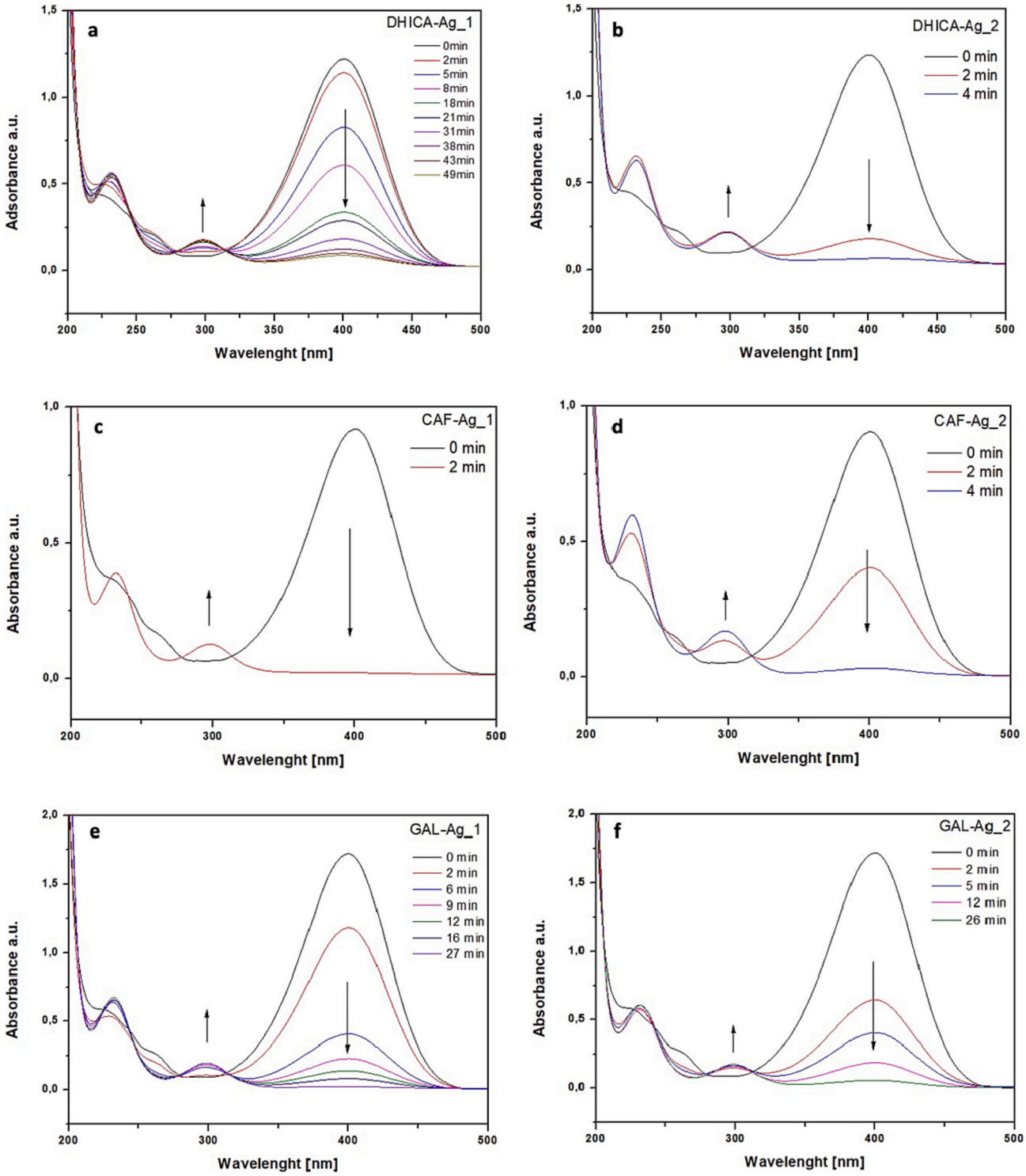


**Fig. 9.** UV–Vis spectra related to the reduction reaction of 4-NP to 4-AP over time.

showed comparable and highly fast reduction times almost reproducible in all reuse cycles. On the contrary, the GAL-Ag_2 sample performed with significantly longer reaction times than the other samples, and the reaction times increased with each reuse cycle. The opposite trend for DHICA-Ag_1 could be attributed to significant morphological changes caused by repeated reaction cycles. Indeed, $NaBH_4$ might cause erosion and debridement of the silicate component, leading to progressive higher exposure of silver domains, as visually described in the Fig. 13. Furthermore, the unique behavior observed in the DHICA-Ag_1 sample can be attributed to structural modifications probably caused by prolonged contact of the nanocatalyst with the reducing agent. In this scenario, the $NaBH_4$ could potentially attack on the silicate component, leading to a gradual increase in external exposure of the metal active sites. Initially, these active sites may have been situated inside the nanoparticles. The schematic representation in the Fig. 13 illustrates this possibility, suggesting that the modification of the silicate structure over time could enhance the accessibility of active metal sites on the surface of the DHICA-Ag_1 sample over time, thereby contributing to its "self-

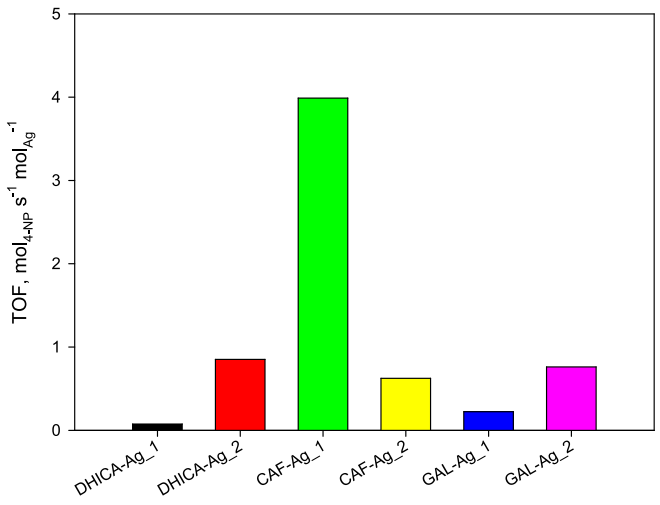


**Fig. 10.** TOFs related to the conversion reaction of 4-NP to 4-AP.

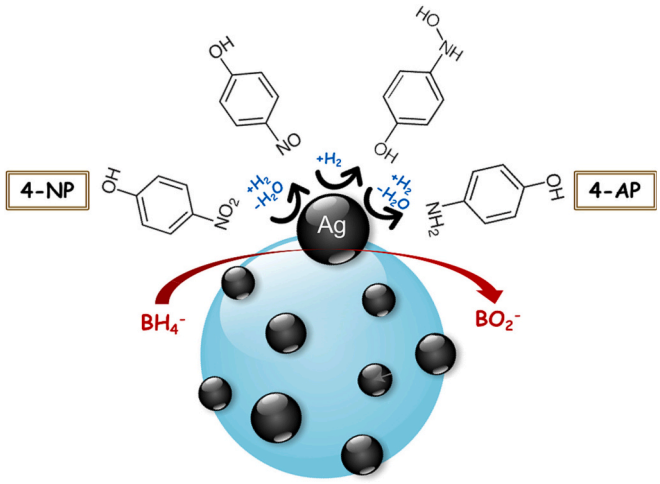


**Fig. 11.** Scheme of the reduction reaction of 4-Nitrophenol and its reduction to 4-Aminophenol.

activation" behavior observed during reuse cycles.

Finally, regarding the GAL-Ag_1 and GAL-Ag_2 samples, as already discussed for the MB degradation reactions, the presence of a smaller number of active metal sites on the surface results in longer reduction times. Furthermore, prolonged interaction with the reducing agent may lead to a loss of the active silver phase in solution, mainly located on the surface of the nanoparticle, resulting in a decrease in catalytic efficiency with time. Indeed, there is a significant increase in the overall reduction times during the reuse cycles for both samples, with the GAL-Ag_2 sample reaching up to 80 min for complete reduction.

## 4. Conclusions

The successful synthesis of hybrid organic-inorganic structures composed of silica and polyphenolic compounds, decorated with metallic silver, has been proposed and effectively tested as biocompatible nanocatalysts for the removal of organic dyes from wastewater. Following a sustainable approach, bio-available caffeic acid and gallic acid were exploited as potential reducing precursors of $Ag^{+}$ to $Ag^{0}$ and the effect of two distinct synthetic methods (procedures 1 and 2) on particle morphologies and functionalities was examined. The results of physical-chemical characterization proved that all phenolic acids reduce silver ions tailoring distribution and size of $Ag^{0}$ domains in the nanostructures. Furthermore, depending on the different synthetic procedure and the nature of phenolic acid, either metal core or surface exposed metal cluster site can result as a final architecture. All proposed systems exhibit impressive adsorption capacity and quick degradation kinetics in the treatment of MB and 4-NP. The samples obtained by procedure 2, where silver nitrate was added to pre-formed hybrid systems, exhibited increased metal site accessibility and were thus found to be the most effective in terms of both MB and 4-NP reduction.

Ultrafine silver nanoparticles with very small sizes (sub nanometer-2 nm) were obtained on the surface of CAF sample from procedure 1,

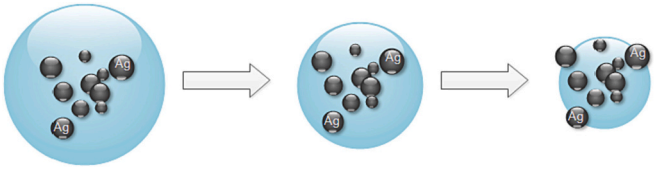


**Fig. 13.** Possible schematic representation of structural evolution of DHICA-Ag_1 sample after pronged contact time with NaBH4.

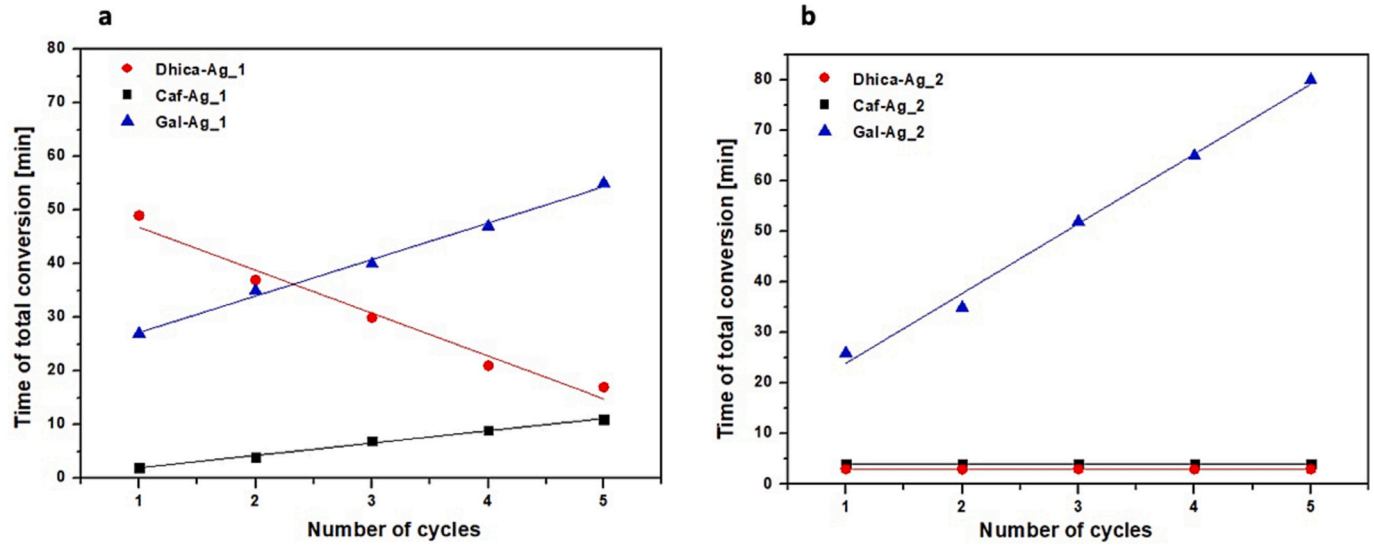


**Fig. 12.** Total 4-NP reduction reaction times versus reuse cycles for samples synthesized by using procedures 1 (a) and procedure 2 (b).

leading to exceptional catalytic activity with the highest TOF value. Moreover, the architecture of the nanocatalysts strongly affects their behavior in reusability experiments, with both DHICA and CAF samples from procedure 2, showing good reusability after even 5 cycles of reuse without decreasing catalytic activity. Careful selection of the suitable polyphenolic precursors and synthesis routes has proven beneficial in modifying the final architecture of the particles and therefore increasing their catalytic activity. Overall, the presented results demonstrate the high potential of these systems for the removal of organic pollutants.

## CRediT authorship contribution statement

**Marianna Orrico:** Methodology, Investigation, Data curation, Conceptualization. **Giulio Pota:** Writing – review & editing, Investigation, Data curation. **Virginia Venezia:** Writing – review & editing, Investigation, Data curation. **Bruno de Gennaro:** Writing – review & editing. **Gianluca Landi:** Writing – review & editing. **Fabiana Tescione:** Writing – review & editing. **Alessandro Pezzella:** Writing – review & editing, Conceptualization. **Giuseppina Luciani:** Writing – review & editing, Supervision, Data curation, Conceptualization. **Brigida Silvestri:** Writing – original draft, Supervision, Project administration, Methodology, Data curation, Conceptualization.

## Declaration of competing interest

The authors declare that they have no known competing financial interests or personal relationships that could have appeared to influence the work reported in this paper.

## Data availability

No data was used for the research described in the article.

## Acknowledgements

The authors thank the European Union (FSE, PON Ricerca e Innovazione 2014–2020, Azione IV.5 “Dottorati di ricerca su tematiche Green”) for funding a XXXVII Cycle Ph.D. grant to Dr. Marianna Orrico.

## Appendix A. Supplementary data

Supplementary data to this article can be found online at https://doi.org/10.1016/j.jwpe.2024.105079.

## References

[1] B.S. Rathi, P.S. Kumar, D.-V.N. Vo, Critical review on hazardous pollutants in water environment: occurrence, monitoring, fate, removal technologies and risk assessment, Sci. Total Environ. 797 (2021) 149134.
[2] S. Samsami, M. Mohamadizaniani, M.-H. Sarrafzadeh, E.R. Rene, M. Firoozbahr, Recent advances in the treatment of dye-containing wastewater from textile industries: overview and perspectives, Process Saf. Environ. Prot. 143 (2020) 138–163.
[3] S. Khan, M. Naushad, M. Govarthanan, J. Iqbal, S.M. Alfadul, Emerging contaminants of high concern for the environment: current trends and future research, Environ. Res. 207 (2022) 112609.
[4] M.A. Kaczorowska, D. Bożejewicz, K. Witt, The application of polymer inclusion membranes for the removal of emerging contaminants and synthetic dyes from aqueous solutions—a mini review, Membranes (Basel) 13 (2023) 132.
[5] J. Singh, P. Gupta, A. Das, Dyes from textile industry wastewater as emerging contaminants in agricultural fields, in: Sustainable Agriculture Reviews 50: Emerging Contaminants in Agriculture, 2021, pp. 109–129.
[6] R. Kishor, D. Purchase, G.D. Saratale, R.G. Saratale, L.F.R. Ferreira, M. Bilal, R. Chandra, R.N. Bharagava, Ecotoxicological and health concerns of persistent coloring pollutants of textile industry wastewater and treatment approaches for environmental safety, J. Environ. Chem. Eng. 9 (2021) 105012.
[7] S. Mani, P. Chowdhary, R.N. Bharagava, Textile wastewater dyes: toxicity profile and treatment approaches, in: Emerging and Eco-Friendly Approaches for Waste Management, 2019, pp. 219–244.
[8] S. Samsami, M. Mohamadizaniani, M.-H. Sarrafzadeh, E.R. Rene, M. Firoozbahr, Recent advances in the treatment of dye-containing wastewater from textile industries: overview and perspectives, Process Saf. Environ. Prot. 143 (2020) 138–163.
[9] F.E. de Sousa Freitas, M.V.P. Rocha, Study of the performance of lignin from cashew apple bagasse (Anarcadium occidentale L) as adsorbent for industrial synthetic dye, J. Environ. Chem. Eng. 11 (2023) 110430.
[10] J. El Gaayda, F.E. Titchou, I. Barra, I. Karmal, H. Afanga, H. Zazou, P.-S. Yap, Z. Z. Abidin, M. Hamdani, R.A. Akbour, Optimization of turbidity and dye removal from synthetic wastewater using response surface methodology: effectiveness of Moringa oleifera seed powder as a green coagulant, J. Environ. Chem. Eng. 10 (2022) 106988.
[11] V. Vinayagam, K.N. Palani, S. Ganesh, S. Rajesh, V.V. Akula, R. Avoodaiappan, O. S. Kushwaha, A. Pugazhendhi, Recent developments on advanced oxidation processes for degradation of pollutants from wastewater with focus on antibiotics and organic dyes, Environ. Res. 240 (2023) 117500.
[12] Q. Song, X. Chen, Y. Hua, S. Chen, L. Ren, X. Dai, Biological treatment processes for saline organic wastewater and related inhibition mechanisms and facilitation techniques: a comprehensive review, Environ. Res. 239 (2023) 117404.
[13] A. George, A.D. Raj, A.A. Irudayaraj, R.L. Josephine, X. Venci, S.J. Sundaram, R. Rajakrishnan, P. Kuppusamy, K. Kaviyarasu, Regeneration study of MB in recycling runs over nickel vanadium oxide by solvent extraction for photocatalytic performance for wastewater treatments, Environ. Res. 211 (2022) 112970.
[14] M. Ahmed, R.K. Alambi, G. Bhadrachari, S. Al-Muqahwi, J.P. Thomas, Design and optimization of a unique pilot scale forward osmosis integrated membrane distillation system for seawater desalination, J. Environ. Chem. Eng. 11 (2023) 109949.
[15] B. Hazarika, M. Ahmaruzzaman, M.S. Santosh, D. Barceló, S. Rtimi, Advances in polymer-based nanocomposite membranes for water remediation: preparation methods, critical issues and mechanisms, J. Environ. Chem. Eng. 11 (2023) 111401.
[16] A. Bashir, A.H. Pandith, A. Qureashi, L.A. Malik, M. Gani, J.M. Perez, Catalytic propensity of biochar decorated with core-shell nZVI@ Fe3O4: a sustainable photo-Fenton catalysis of methylene blue dye and reduction of 4-nitrophenol, J. Environ. Chem. Eng. 10 (2022) 107401.
[17] K. Saravanan, B. Shanthi, C. Ravichandran, B. Venkatachalapathy, K. I. Sathiyanarayanan, S. Rajendran, N.S. Karthikeyan, R. Suresh, Transformation of used aluminium foil food container into AlOOH nanoflakes with high catalytic activity in anionic azo dye reduction, Environ. Res. 218 (2023) 114985.
[18] A. Ehsani, S. Nejatbakhsh, A.M. Soodmand, M.E. Farshchi, H. Aghdasinia, High-performance catalytic reduction of 4-nitrophenol to 4-aminophenol using M-BDC (M= Ag, Co, Cr, Mn, and Zr) metal-organic frameworks, Environ. Res. 227 (2023) 115736.
[19] S.H. Teo, C.H. Ng, A. Islam, G. Abdulkareem-Alsultan, C.G. Joseph, J. Janaun, Y. H. Taufiq-Yap, S. Khandaker, G.J. Islam, H. Znad, Sustainable toxic dyes removal with advanced materials for clean water production: a comprehensive review, J. Clean. Prod. 332 (2022) 130039.
[20] R.M. Waliullah, A.I. Rehan, M.E. Awual, A.I. Rasee, M.C. Sheikh, M.S. Salman, M. S. Hossain, M.M. Hasan, K.T. Kubra, M.N. Hasan, Optimization of toxic dye removal from contaminated water using chitosan-grafted novel nanocomposite adsorbent, J. Mol. Liq. 388 (2023) 122763.
[21] F. Amalina, A.S. Abd Razak, S. Krishnan, A.W. Zularisam, M. Nasrullah, Dyes removal from textile wastewater by agricultural waste as an absorbent–a review, Clean. Waste Syst. 3 (2022) 100051.
[22] D. Vishnu, B. Dhandapani, A review on the synergetic effect of plant extracts on nanomaterials for the removal of metals in industrial effluents, Curr. Anal. Chem. 17 (2021) 260–271.
[23] H. Veisi, S. Razeghi, P. Mohammadi, S. Hemmati, Silver nanoparticles decorated on thiol-modified magnetite nanoparticles (Fe3O4/SiO2-Pr-S-Ag) as a recyclable nanocatalyst for degradation of organic dyes, Mater. Sci. Eng. C 97 (2019) 624–631.
[24] D. Lan, H. Zhu, J. Zhang, S. Li, Q. Chen, C. Wang, T. Wu, M. Xu, Adsorptive removal of organic dyes via porous materials for wastewater treatment in recent decades: a review on species, mechanisms and perspectives, Chemosphere 293 (2022) 133464.
[25] S. Marimuthu, A.J. Antonisamy, S. Malayandi, K. Rajendran, P.C. Tsai, A. Pugazhendhi, V.K. Ponnusamy, Silver nanoparticles in dye effluent treatment: a review on synthesis, treatment methods, mechanisms, photocatalytic degradation, toxic effects and mitigation of toxicity, J. Photochem. Photobiol. B 205 (2020) 111823, https://doi.org/10.1016/J.JPHOTOBIOL.2020.111823.
[26] B.S. Damasceno, A.F.V. Da Silva, A.C.V. De Araújo, Dye adsorption onto magnetic and superparamagnetic Fe3O4 nanoparticles: a detailed comparative study, J. Environ. Chem. Eng. 8 (2020) 103994, https://doi.org/10.1016/J.JECE.2020.103994.
[27] M.P. Ajith, M. Aswathi, E. Priyadarshini, P. Rajamani, Recent innovations of nanotechnology in water treatment: a comprehensive review, Bioresour. Technol. 342 (2021) 126000, https://doi.org/10.1016/J.BIORTECH.2021.126000.
[28] C. Osagie, A. Othmani, S. Ghosh, A. Malloum, Z. Kashitarash Esfahani, S. Ahmadi, Dyes adsorption from aqueous media through the nanotechnology: a review, J. Mater. Res. Technol. 14 (2021) 2195–2218, https://doi.org/10.1016/J.JMRT.2021.07.085.
[29] H. Xu, B. Liu, M. Zhang, Synthesis of silver nanoparticles composite mesoporous microspheres for synergistic adsorption-catalytic degradation of methylene blue, Sep. Purif. Technol. 324 (2023) 124499, https://doi.org/10.1016/J.SEPPUR.2023.124499.
[30] J. Fang, Q. Diao, M. Chen, S. Zhao, Y. Li, K. Wei, Z. Huang, Q. Zhuo, Rational fabrication of Ti0.69Zr0.31O2 modified Au-loaded halloysite core-shell catalyst for highly efficient reduction of 4-nitrophenol and dye pollutants, Colloids Surf. A

Physicochem. Eng. Asp. 677 (2023) 132305, https://doi.org/10.1016/J.COLSURFA.2023.132305.
[31] Z. Yang, X. Liu, S. Xia, Q. Ding, H. Liu, Z. Wang, L. Zhang, H. Zhang, Au/Boron organic frameworks for efficient removal and degradation of azo dye pollutants, Colloids Surf. A Physicochem. Eng. Asp. 646 (2022) 128884, https://doi.org/10.1016/J.COLSURFA.2022.128884.
[32] S. Aslam, F. Subhan, Z. Liu, Z. Yan, A. Ahmad, A. Nazir, A. Siddiqa, M. Yaseen, Magnetic Fe3O4@MIL-100(Fe) core-shells decorated with gold nanoparticles for enhanced catalytic reduction of 4-nitrophenol and degradation of azo dye, Colloids Surf. A Physicochem. Eng. Asp. 660 (2023) 130904, https://doi.org/10.1016/J.COLSURFA.2022.130904.
[33] M. Parmar, M. Sanyal, Extensive study on plant mediated green synthesis of metal nanoparticles and their application for degradation of cationic and anionic dyes, Environ. Nanotechnol. Monit. Manag. 17 (2022) 100624, https://doi.org/10.1016/J.ENMM.2021.100624.
[34] N.T. Nandhini, S. Rajeshkumar, S. Mythili, The possible mechanism of eco-friendly synthesized nanoparticles on hazardous dyes degradation, Biocatal. Agric. Biotechnol. 19 (2019) 101138, https://doi.org/10.1016/J.BCAB.2019.101138.
[35] T.N.J.I. Edison, R. Atchudan, N. Karthik, J. Balaji, D. Xiong, Y.R. Lee, Catalytic degradation of organic dyes using green synthesized N-doped carbon supported silver nanoparticles, Fuel 280 (2020) 118682, https://doi.org/10.1016/J.FUEL.2020.118682.
[36] R. Edge, M. D'Ischia, E.J. Land, A. Napolitano, S. Navaratnam, L. Panzella, A. Pezzella, C.A. Ramsden, P.A. Riley, Dopaquinone redox exchange with dihydroxyindole and dihydroxyindole carboxylic acid, Pigment Cell Res. 19 (2006) 443–450, https://doi.org/10.1111/J.1600-0749.2006.00327.X.
[37] N.T.T. Nguyen, T.T.T. Nguyen, D.T.C. Nguyen, T. Van Tran, Green synthesis of ZnFe2O4 nanoparticles using plant extracts and their applications: a review, Sci. Total Environ. 872 (2023) 162212, https://doi.org/10.1016/J.SCITOTENV.2023.162212.
[38] M. Ahani, M. Khatibzadeh, Green synthesis of silver nanoparticles using gallic acid as reducing and capping agent: effect of pH and gallic acid concentration on average particle size and stability, Inorg. Nano-Met. Chem. 52 (2022) 234–240, https://doi.org/10.1080/24701556.2021.1891428.
[39] C. Thummaneni, D.V. Surya Prakash, R. Golli, M. Vangalapati, Green synthesis of silver nanoparticles and characterization of caffeic acid from Myristica fragrans (Nutmeg) against antibacterial activity, Mater. Today Proc. 62 (2022) 4001–4005, https://doi.org/10.1016/J.MATPR.2022.04.586.
[40] S. Ahmad, S. Munir, N. Zeb, A. Ullah, B. Khan, J. Ali, M. Bilal, M. Omer, M. Alamzeb, S.M. Salman, S. Ali, Green nanotechnology: a review on green synthesis of silver nanoparticles — an ecofriendly approach, Int. J. Nanomedicine 14 (2019) 5087–5107, https://doi.org/10.2147/IJN.S200254.
[41] V.P. Aswathi, S. Meera, C.G.A. Maria, M. Nidhin, Green synthesis of nanoparticles from biodegradable waste extracts and their applications: a critical review, Nanotechnol. Environ. Eng. 8 (2) (2022) 377–397, https://doi.org/10.1007/S41204-022-00276-8.
[42] M. Sohail Latif, M. Kamarulzaki Mustafa, Green Synthesis of Plant-Mediated Metal Nanoparticles: The Role of Polyphenols, 2019, p. 12, https://doi.org/10.22159/ajpcr.2019.v12i7.33211.
[43] B.A. Omran, K.H. Baek, Valorization of agro-industrial biowaste to green nanomaterials for wastewater treatment: approaching green chemistry and circular economy principles, J. Environ. Manag. 311 (2022) 114806, https://doi.org/10.1016/J.JENVMAN.2022.114806.
[44] S. Eghbaliferiz, M. Iranshahi, Prooxidant activity of polyphenols, flavonoids, anthocyanins and carotenoids: updated review of mechanisms and catalyzing metals, Phytother. Res. 30 (2016) 1379–1391, https://doi.org/10.1002/PTR.5643.
[45] K. Yoosaf, B. Itty Ipe, C.H. Suresh, K. George Thomas, In situ synthesis of metal nanoparticles and selective naked-eye detection of lead ions from aqueous media, J. Phys. Chem. C 111 (2007) 12839–12847, https://doi.org/10.1021/jp073923q.
[46] M. Apte, G. Girme, A. Bankar, A. RaviKumar, S. Zinjarde, 3, 4-Dihydroxy-L-phenylalanine-derived melanin from Yarrowia lipolytica mediates the synthesis of silver and gold nanostructures, J. Nanobiotechnol. 11 (2013) 2, https://doi.org/10.1186/1477-3155-11-2.
[47] V. Venezia, M. Verrillo, N. Gallucci, R. Di Girolamo, G. Luciani, G. D'Errico, L. Paduano, A. Piccolo, G. Vitiello, Exploiting biodervied humic acids: a molecular combination with ZnO nanoparticles leads to nanostructured hybrid interfaces with enhanced pro-oxidant and antibacterial activity, J. Environ. Chem. Eng. 11 (2023) 108973, https://doi.org/10.1016/J.JECE.2022.108973.
[48] G. Pota, B. Silvestri, G. Vitiello, N. Gallucci, R. Di Girolamo, S. Scialla, M.G. Raucci, L. Ambrosio, M. Di Napoli, A. Zanfardino, Towards nanostructured red-ox active bio-interfaces: bioinspired antibacterial hybrid melanin-CeO2 nanoparticles for radical homeostasis, Biomater. Adv. 153 (2023) 213558.
[49] B. Silvestri, P. Armanetti, G. Pota, G. Vitiello, A. Pezzella, L. Menichetti, V. Giannini, G. Luciani, Enhanced photoacoustic response by synergistic ag–melanin interplay at the core of ternary biocompatible hybrid silica-based nanoparticles, ACS Appl. Mater. Interfaces 15 (2023) 46756–46764.
[50] B. Silvestri, P. Armanetti, G. Sanità, G. Vitiello, A. Lamberti, G. Calì, A. Pezzella, G. Luciani, L. Menichetti, S. Luin, Silver-nanoparticles as plasmon-resonant enhancers for eumelanin's photoacoustic signal in a self-structured hybrid nanoprobe, Mater. Sci. Eng. C 102 (2019) 788–797.
[51] B. Silvestri, G. Vitiello, G. Luciani, V. Calcagno, A. Costantini, M. Gallo, S. Parisi, S. Paladino, M. Iacomino, G. D'Errico, M.F. Caso, A. Pezzella, M. D'Ischia, Probing the eumelanin-silica interface in chemically engineered bulk hybrid nanoparticles for targeted subcellular antioxidant protection, ACS Appl. Mater. Interfaces 9 (2017) 37615–37622, https://doi.org/10.1021/acsami.7b11839.
[52] F. Tescione, O. Tammaro, A. Bifulco, G. Del Monaco, S. Esposito, M. Pansini, B. Silvestri, A. Costantini, Silica meets tannic acid: designing green nanoplatforms for environment preservation, Molecules 27 (2022) 1944, https://doi.org/10.3390/molecules27061944.
[53] P. Russo, A. Costantini, G. Luciani, F. Tescione, M. Lavorgna, F. Branda, B. Silvestri, Thermo-mechanical behavior of poly (butylene terephthalate)/silica nanocomposites, J. Appl. Polym. Sci. 135 (2018) 46006.
[54] X. Zhang, H. Sun, S. Tan, J. Gao, Y. Fu, Z. Liu, Hydrothermal synthesis of Ag nanoparticles on the nanocellulose and their antibacterial study, Inorg. Chem. Commun. 100 (2019) 44–50, https://doi.org/10.1016/J.INOCHE.2018.12.012.
[55] N. Swilam, K.A. Nematallah, Polyphenols profile of pomegranate leaves and their role in green synthesis of silver nanoparticles, Sci. Rep. 10 (2020), https://doi.org/10.1038/s41598-020-71847-5.
[56] Y. Li, Y. Chen, P. Li, G. Wang, J. Wei, Controllable deposition of Ag nanoparticles on various substrates via interfacial polyphenol reduction strategy for antibacterial application, Colloids Surf. A Physicochem. Eng. Asp. 655 (2022) 130287, https://doi.org/10.1016/J.COLSURFA.2022.130287.
[57] G. Pota, G. Vitiello, V. Venezia, F. Della Sala, A. Borzacchiello, A. Costantini, L. Paduano, L.P. Cavalcanti, F. Tescione, B. Silvestri, G. Luciani, Shall we tune? From core-shell to cloud type nanostructures in heparin/silica hybrids, Polymers (Basel) 14 (2022), https://doi.org/10.3390/polym14173568.
[58] V. Venezia, A. Costantini, G. Landi, A. Di Benedetto, F. Sannino, V. Califano, Immobilization of β-glucosidase over structured cordierite monoliths washcoated with wrinkled silica nanoparticles, Catalysts 10 (2020) 889.
[59] B. Silvestri, D. Guarnieri, G. Luciani, A. Costantini, P.A. Netti, F. Branda, Fluorescent (rhodamine), folate decorated and doxorubicin charged, PEGylated nanoparticles synthesis, J. Mater. Sci. Mater. Med. 23 (2012) 1697–1704, https://doi.org/10.1007/s10856-012-4634-2.
[60] M. Hu, X. Yan, X. Hu, R. Feng, M. Zhou, Synthesis of silver decorated silica nanoparticles with rough surfaces as adsorbent and catalyst for methylene blue removal, J. Sol-Gel Sci. Technol. 89 (2019) 754–763, https://doi.org/10.1007/s10971-018-4871-z.
[61] A.N. Chishti, F. Guo, A. Aftab, Z. Ma, Y. Liu, M. Chen, J. Gautam, C. Chen, L. Ni, G. Diao, Synthesis of silver doped Fe3O4/C nanoparticles and its catalytic activities for the degradation and reduction of methylene blue and 4-nitrophenol, Appl. Surf. Sci. 546 (2021) 149070, https://doi.org/10.1016/J.APSUSC.2021.149070.
[62] A. Elfiad, F. Galli, L.M. Boukhobza, A. Djadoun, D.C. Boffito, Low-cost synthesis of Cu/α-Fe2O3 from natural HFeO2: application in 4-nitrophenol reduction, J. Environ. Chem. Eng. 8 (2020) 104214, https://doi.org/10.1016/J.JECE.2020.104214.
[63] K. Wang, R. Chen, X. Zhu, Q. Liao, D. Ye, G. Chen, M. Liu, Simple method for directly synthesizing Ag nanoparticles with silver ammonia and polydopamine in a microreactor toward the conversion of 4-NP to 4-AP, Ind. Eng. Chem. Res. 59 (2020) 16205–16216, https://doi.org/10.1021/acs.iecr.0c03117.
[64] D. Das, R. Sarkar, S. Mukherjee, K.K. Chattopadhyay, Sodium borohydride assisted reduction of toxic pollutants by silver coordinated melamine based polymeric material, Mater. Today Proc. 44 (2021) 444–452, https://doi.org/10.1016/J.MATPR.2020.09.755.